GEOPHYSICS, VOL. 68, NO. 3 (MAY-JUNE 2003); P. 1022–1031, 11 FIGS., 1 TABLE.
10.1190/1.1581073

Inversion of multicomponent, multiazimuth, walkaway VSP data for the stiffness tensor

Pawan Dewangan* and Vladimir Grechka‡

ABSTRACT

Vertical seismic profiling (VSP), an established technique, can be used for estimating in-situ anisotropy that might provide valuable information for characterization of reservoir lithology, fractures, and fluids. The P-wave slowness components, conventionally measured in multiazimuth, walkaway VSP surveys, allow one to reconstruct some portion of the corresponding slowness surface. A major limitation of this technique is that the P-wave slowness surface alone does not constrain a number of stiffness coefficients that may be crucial for inferring certain rock properties. Those stiffnesses can be obtained only by combining the measurements of P-waves with those of S (or PS) modes.

Here, we extend the idea of Horne and Leaney, who proved the feasibility of joint inversion of the slowness and polarization vectors of P- and SV-waves for parameters of transversely isotropic media with a vertical symmetry axis (VTI symmetry). We show that there is no need to assume a priori VTI symmetry or any other specific type of anisotropy. Given a sufficient polar and azimuthal coverage of the data, the polarizations and slownesses of P and two split shear (S1 and S2) waves are sufficient for estimating all 21 elastic stiffness coefficients c_{ij} that characterize the most general triclinic anisotropy. The inverted stiffnesses themselves indicate whether or not the data can be described by a higher-symmetry model.

We discuss three different scenarios of inverting noise-contaminated data. First, we assume that the layers are horizontal and laterally homogeneous so that the horizontal slownesses measured at the surface are preserved at the receiver locations. This leads to a linear inversion scheme for the elastic stiffness tensor **c**. Second, if the S-wave horizontal slowness at the receiver location is unknown, the elastic tensor **c** can be estimated in a nonlinear fashion simultaneously with obtaining the horizontal slowness components of S-waves. The third scenario includes the nonlinear inversion for **c** using only the vertical slowness components and the polarization vectors of P- and S-waves. We find the inversion to be stable and robust for the first and second scenarios. In contrast, errors in the estimated stiffnesses increase substantially when the horizontal slowness components of both P- and S-waves are unknown. We apply our methodology to a multiazimuth, multicomponent VSP data set acquired in Vacuum field, New Mexico, and show that the medium at the receiver level can be approximated by an azimuthally rotated orthorhombic model.

INTRODUCTION

Multiazimuth walkaway vertical seismic profiling (VSP) can be used for measuring in-situ anisotropy. It is usually estimated from P-wave slowness surfaces $\mathbf{p}^{(P)}$ (e.g., Gaiser, 1990; Miller and Spencer, 1994) constructed by differentiating the traveltimes $t^{(P)}$ of the first arrivals with respect to the coordinates $\mathbf{x}$ of the surface sources and the downhole geophones, $p_i^{(P)} = \partial t^{(P)}/\partial x_i (i = 1, 2, 3)$. Because of the acquisition geometry, the vertical slowness components $p_3^{(P)}$ are obtained only at the geophone levels, whereas the horizontal components $p_1^{(P)}$ and $p_2^{(P)}$ are computed only at the earth's surface. To reconstruct the slowness surfaces in the borehole, one usually assumes lateral homogeneity of the overburden. Then, according to Snell's law, the horizontal slownesses $p_1^{(P)}$ and $p_2^{(P)}$ are preserved along any ray travelling from sources to downhole receivers. Although the presence of even mild lateral velocity variations is known to lead to noticeable distortions of the reconstructed slowness surfaces and, consequently, to substantial

Manuscript received by the Editor June 24, 2002; revised manuscript received October 30, 2002.
*Colorado School of Mines, Center for Wave Phenomena, 924 16th Street, Green Center Building, Golden, Colorado 80401. E-mail: pdewanga@dix.mines.edu.
‡Formerly Colorado School of Mines, Center for Wave Phenomena, Golden, Colorado 80401; presently Shell International Exploration and Production, 3737 Bellaire Boulevard, Post Office Box 481, Houston, Texas 77001-0481. E-mail: Vladimir.Grechka@shell.com.

errors in the estimated anisotropic parameters (Gaiser, 1990; Sayers, 1997), Bakulin et al. (2000c) found a practical way of correcting the slownesses for lateral heterogeneity of the overburden. Still, P-wave slowness surfaces $\mathbf{p}^{(P)}$ are inherently insufficient for constraining several stiffness coefficients needed for describing certain rock properties (e.g., Zheng and Pšenčík, 2002). Combining P- and S-wave VSP data is necessary for a more comprehensive reservoir characterization.

In general, three-component geophones are required to record S-waves at oblique incidence and perform Alford-type rotation to separate the fast (S_1) and slow (S_2) shear-wave arrivals (Dellinger et al., 2001). In addition to the S_1- and S_2-wave traveltimes (which can be differentiated in the same manner as those of P-waves to obtain the slownesses), Alford rotation results in the polarization vectors $\mathbf{A}^{(S_1)}$ and $\mathbf{A}^{(S_2)}$ of the split shear waves. Since the polarizations are measured locally at the geophones, they can be used, along with the slownesses, for anisotropic parameter estimation. Horne and Leaney (2000) recognized this possibility and developed a procedure for joint inversion of P- and SV-wave VSP data for parameters of transversely isotropic media with a vertical symmetry axis (VTI). The VTI model, however, might be too simplistic for characterization of realistic reservoirs. For instance, dipping beds lead to tilted transverse isotropy (TTI model), whereas the presence of vertical fractures might reduce the symmetry of effective media to orthorhombic, monoclinic, or even triclinic (Bakulin et al., 2000a,b; Grechka et al., 2001). Although, some anisotropic coefficients can be found from reflection seismics, in general it is impossible to estimate all quantities needed for reservoir characterization from surface data. Thus, it is important to examine whether or not multicomponent, multiazimuth, walkaway VSP data can be used to obtain parameters of lower-symmetry anisotropic media.

Here we show that all 21 stiffness coefficients can be found given a sufficient polar and azimuthal coverage of the data. Errors in their values turn out to depend on the complexity of the overburden, which determines our ability to use the horizontal slowness components (measured at the surface) in the inversion. We consider three possible scenarios for the inversion of VSP data.

Scenario 1. The overburden is close to horizontally layered (Figure 1a), and lateral velocity variations of P- and S-waves are known, for instance, from surface seismics. The expense of shear-wave excitation can be avoided by obtaining the S modes from converted (PS) wave reflections. The possible influence of lateral velocity heterogeneity on the horizontal slowness components of P- and S-waves might be corrected by applying the technique described by Bakulin at al. (2000c). With such a correction, local values of the slowness vectors $\mathbf{p}^{(P)}$, $\mathbf{p}^{(S_1)}$, and $\mathbf{p}^{(S_2)}$ and the polarizations $\mathbf{A}^{(P)}$, $\mathbf{A}^{(S_1)}$, and $\mathbf{A}^{(S_2)}$ of all three modes are available at the receiver locations and can be used to estimate the elastic stiffness coefficients c_{ij}. This results in a linear inverse problem for the tensor $\mathbf{c}$ [see equations (1) below].

Scenario 2. It may happen that only conventional P-wave surface seismic data were acquired and the S-wave velocity distribution is unknown, or shear waves recorded by the downhole receivers correspond to PS-wave reflections from dipping interfaces (Figure 1b). In both cases, the horizontal slowness components $p_1^{(S_1)}$, $p_2^{(S_1)}$, and $p_1^{(S_2)}$, $p_2^{(S_2)}$ of S-waves are, in general, unknown at receiver locations. The tensor $\mathbf{c}$, however, can still be estimated by inverting the slownesses $\mathbf{p}^{(P)}$, $p_3^{(S_1)}$, and $p_3^{(S_2)}$ and the polarization vectors $\mathbf{A}^{(P)}$, $\mathbf{A}^{(S_1)}$, and $\mathbf{A}^{(S_2)}$. The inversion becomes nonlinear in this case.

Scenario 3. If the subsurface is so complicated that it is impossible to obtain the horizontal slownesses of both P- and S-waves at the receiver locations (Figure 1c), only the quantities $p_3^{(P)}$, $p_3^{(S_1)}$, $p_3^{(S_2)}$, and $\mathbf{A}^{(P)}$, $\mathbf{A}^{(S_1)}$, $\mathbf{A}^{(S_2)}$ comprise the input for estimating the tensor $\mathbf{c}$. The inversion problem is again nonlinear.

Below, we analyze these three inversion scenarios and apply the developed procedure to estimate the elastic stiffness tensor $\mathbf{c}$ for a multiazimuth, multicomponent VSP data set acquired in Vacuum field, New Mexico.

ANALYTIC BACKGROUND

The forward model for the inverse problem at hand is simply the Christoffel equation, which determines the polarization

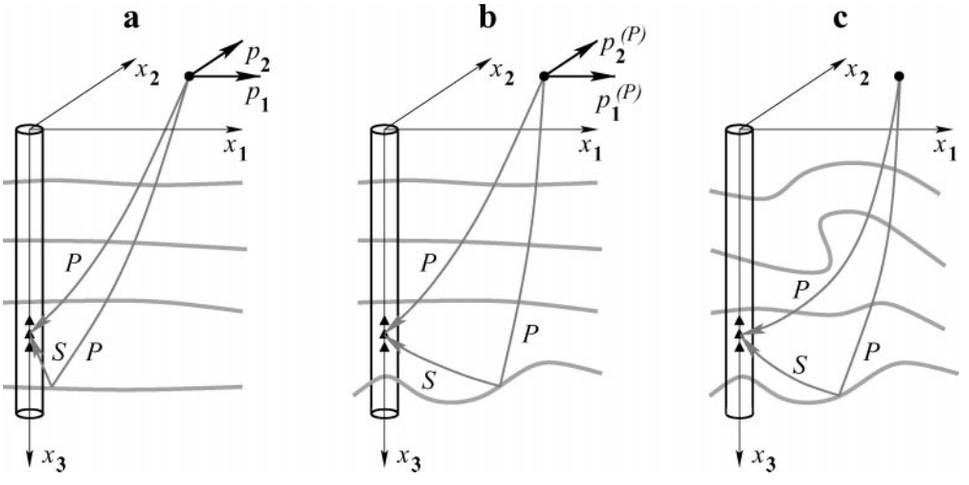

FIG. 1. Three different scenarios of the inversion of multicomponent VSP data corresponding to different levels of the complexity of the subsurface: (a) scenario 1, (b) scenario 2, and (c) scenario 3.

and slowness vectors of plane waves propagating in anisotropic media (e.g., Tsvankin, 2001):

$$F_k^{(Q)} \equiv G_{k\ell'}^{(Q)} A_{\ell'}^{(Q)} - A_k^{(Q)} = 0, \tag{1}$$

where

$$G_{k\ell'}^{(Q)} = c_{kk'\ell\ell'} p_{k'}^{(Q)} p_{\ell}^{(Q)}, \tag{2}$$

$$(Q = \mathrm{P},\ \mathrm{S}_1,\ \mathrm{S}_2;\ k = 1,\ 2,\ 3).$$

As in typical notation, we require the polarization vectors $\mathbf{A}^{(Q)}$ to be normalized, $|\mathbf{A}^{(Q)}| = 1$, define the wave type according to inequality $|\mathbf{p}^{(P)}| < |\mathbf{p}^{(S_1)}| \le |\mathbf{p}^{(S_2)}|$, and assume summation over all repeated indexes from 1 to 3. The density-normalized stiffness tensor **c**, as well as the vectors **p** and **A**, are defined in a Cartesian coordinate frame with the positive x_3-axis pointing downward. Our goal is to estimate the elastic stiffness tensor **c** by inverting equations (1). In the discussion below, we often use Voigt convention for the components of **c**:

$$c_{kk'\ell\ell'} \to c_{ij} = c_{ji},$$

where the correspondences $kk' \to i$ and $\ell\ell' \to j$ are given by the template

$$i = k\delta_{kk'} + (9 - k - k')(1 - \delta_{kk'}).$$

Here, $\delta_{kk'} = 1$ if $k = k'$ and $\delta_{kk'} = 0$ otherwise. The indexes i and j in Voigt notation change from 1 to 6 indicating that the maximum number of independent components of symmetric tensor **c** is 21.

Scenario 1. If the slowness and polarizations vectors ($\mathbf{p}^{(Q)}$ and $\mathbf{A}^{(Q)}$) of all three modes are measured for N propagation directions, the only unknown in equations (1) is the tensor **c**. Thus, the model and data vectors for scenario 1 are given by

$$\mathbf{m} = \mathbf{c}, \quad \mathbf{d} = \left\{\mathbf{p}_n^{(Q)},\ \mathbf{A}_n^{(Q)}\right\}, \qquad (Q = \mathrm{P},\ \mathrm{S}_1,\ \mathrm{S}_2;\ n = 1, \ldots, N). \tag{3}$$

Clearly, obtaining **c** from equations (1) is a linear inverse problem.

Scenario 2. When the horizontal slowness components of shear waves cannot be measured, the model and data vectors are

$$\mathbf{m} = \left\{\mathbf{c},\ p_{1,n}^{(S_1)},\ p_{2,n}^{(S_1)},\ p_{1,n}^{(S_2)},\ p_{2,n}^{(S_2)}\right\},$$
$$\mathbf{d} = \left\{\mathbf{p}_n^{(P)},\ p_{3,n}^{(S_1)},\ p_{3,n}^{(S_2)},\ \mathbf{A}_n^{(Q)}\right\}, \tag{4}$$
$$(Q = \mathrm{P},\ \mathrm{S}_1,\ \mathrm{S}_2;\ n = 1, \ldots, N).$$

Since the slowness components $p_{i,n}^{(S_1)}$ and $p_{i,n}^{(S_2)}$ ($i = 1,\ 2$) have to be estimated along with the components of the tensor **c**, the inversion becomes nonlinear.

Scenario 3. Finally, when the horizontal slownesses of both P- and S-waves are unknown, we operate with the model and data vectors

$$\mathbf{m} = \left\{\mathbf{c},\ p_{1,n}^{(Q)},\ p_{2,n}^{(Q)}\right\}, \quad \mathbf{d} = \left\{p_{3,n}^{(Q)},\ \mathbf{A}_n^{(Q)}\right\}, \qquad (Q = \mathrm{P},\ \mathrm{S}_1,\ \mathrm{S}_2;\ n = 1, \ldots, N), \tag{5}$$

and the inversion procedure is again nonlinear.

To illustrate the increase in the number of unknowns from scenario 1 to scenario 3, let us assume that there are $N = 30$ spatial directions (data points) specified by a particular azimuth and polar angle, where the polarizations and slownesses of all three modes are measured. In scenario 1, the unknowns are the 21 stiffness coefficients c_{ij} for the most general triclinic anisotropy. In scenario 2, four unknown slowness components $p_1^{(S_1)}, p_2^{(S_1)}, p_1^{(S_2)}, p_2^{(S_2)}$ for each data point [equations (4)] have to be added, increasing the number of unknowns to $21 + (30 \times 4) = 141$. Similarly, in scenario 3 the total number of unknowns becomes $21 + (30 \times 6) = 201$ because the horizontal slownesses of all three modes are unknown [equations (5)].

In general, we have three equations (1) for each mode, so there are nine equations for each data point. Therefore, the total number of equations is $30 \times 9 = 270$. For noise-free, noncontradictory data, however, this number reduces to $30 \times 6 = 180$ exactly at the solution **c** because the components of slowness vectors $\mathbf{p}^{(Q)}$ also satisfy the equality

$$\det\left(c_{kk'\ell\ell'} p_{k'}^{(Q)} p_{\ell}^{(Q)} - \delta_{k\ell'}\right) = 0$$

which makes the polarization vectors $\mathbf{A}^{(Q)}$ the eigenvectors of matrix $\mathbf{G}^{(Q)}$ [equation (2)]. As a consequence, one of three equations (1) can be expressed in terms of the other two. The numbers of independent equations and unknowns are summarized in Table 1. Clearly, the inversion procedure in scenario 3 is underdetermined.

FEASIBILITY OF ESTIMATING STIFFNESS COEFFICIENTS FROM WALKAWAY VSP DATA

In general, our ability to estimate a certain stiffness coefficient depends on the acquisition geometry. If, for instance, all ray trajectories in the data are close to the vertical, the stiffness coefficients c_{11}, c_{12}, c_{22}, and c_{66}, which largely govern wave propagation in near-horizontal directions, will be poorly constrained. The feasibility of estimating a particular stiffness coefficient can be evaluated by examining the Christoffel equation (1) written in the form

$$\mathbf{F}(\mathbf{m},\ \mathbf{d}) = 0, \tag{6}$$

where **m** and **d** are the model and data vectors for the inversion scenarios given by equations (3–5). Then, the model and data perturbations relate as

$$\frac{\partial \mathbf{F}}{\partial \mathbf{m}} \Delta\mathbf{m} + \frac{\partial \mathbf{F}}{\partial \mathbf{d}} \Delta\mathbf{d} = 0. \tag{7}$$

Therefore,

$$\Delta\mathbf{d} = \boldsymbol{\mathcal{F}} \Delta\mathbf{m}, \tag{8}$$

Table 1. Comparison of the numbers of equations and unknowns for a hypothetical VSP data set containing 30 points. Scenarios 1, 2, and 3 are illustrated in Figure 1.

	Number of unknowns		
Number of equations	Scenario 1	Scenario 2	Scenario 3
270 (180)	21	141	201

where the matrix

$$\boldsymbol{\mathcal{F}} = -\left(\frac{\partial \mathbf{F}}{\partial \mathbf{d}}\right)^{\dagger} \frac{\partial \mathbf{F}}{\partial \mathbf{m}} \tag{9}$$

has the meaning of the Frechèt derivative matrix, and † denotes the pseudoinverse.

Using the singular value decomposition (SVD) of the Frechèt matrix, we obtain

$$\boldsymbol{\mathcal{F}} = \mathbf{U}\mathbf{S}\mathbf{V}^{T}. \tag{10}$$

Here **U** and **V** are the eigenvector matrices in the data and model spaces, respectively, **S** is the diagonal matrix of singular values, and T denotes transposition. To get some understanding of how errors in data propagate into the estimated stiffness coefficients, let us assume that the data are contaminated by uncorrelated Gaussian noise that has the standard deviation $\sigma(\mathbf{d}) =$ constant and calculate the standard deviation $\sigma(\mathbf{m})$ of the model vector **m**. The result is (e.g., Press et al., 1987)

$$\sigma_j^2(\mathbf{m}) = \sum_{i=1}^{\dim(\mathbf{d})} \left(\frac{V_{ji}}{S_i}\right)^2 \sigma^2(\mathbf{d}), \quad (j = 1, \ldots, \dim(\mathbf{m})), \tag{11}$$

where V_{ji} is the model eigenvector, S_i is the corresponding singular value, and dim(**a**) denotes the length of vector **a**.

Figure 2 shows typical distribution of errors in the stiffness coefficients inverted following scenario 2. The triclinic model and spatial directions corresponding to 30 data points used in this example are described in the caption of Figure 2. We observe that the errors in different components of the tensor **c** vary. The reason is the limited polar coverage of the data. Since the maximum of the polar angle $\alpha^{(1)}$ is 65° from the vertical, the greatest error-amplification factors are associated with the stiffness coefficients c_{11} and c_{22} that determine the P-wave slownesses and polarizations in directions close to the horizontal. In contrast, the stiffnesses c_{44} and c_{55}, which govern shear-wave signatures near the vertical, are among the best constrained; their error-amplification factors are much smaller.

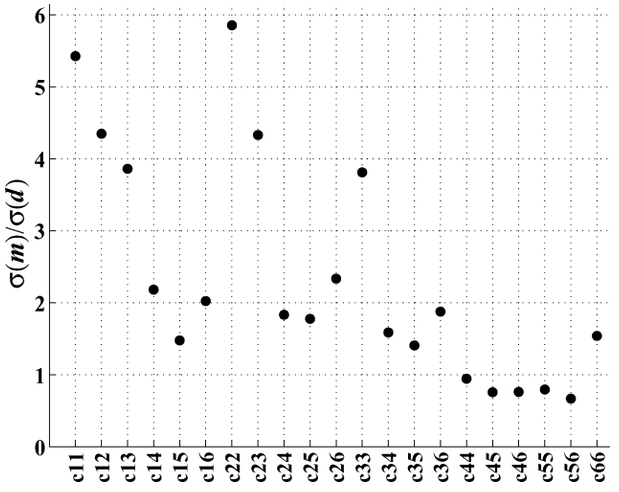

FIG. 2. Error-amplification factors $\sigma(\mathbf{m})/\sigma(\mathbf{d})$ for the stiffnesses c_{ij} computed using equation (11). The spatial directions used to generate the data are specified by five polar angles $\alpha^{(1)} = [13°, 26°, 39°, 52°, 65°]$ and six azimuths $\alpha^{(2)} = [0°, 30°, 60°, 90°, 120°, 150°]$. The model is described by the following density-normalized stiffness coefficients (in km^2/s^2): $c_{11} = 4.00$, $c_{12} = 2.06$, $c_{13} = 2.10$, $c_{14} = -0.05$, $c_{15} = 0.01$, $c_{16} = -0.02$, $c_{22} = 3.83$, $c_{23} = 1.96$, $c_{24} = 0.12$, $c_{25} = -0.05$, $c_{26} = 0.13$, $c_{33} = 3.96$, $c_{34} = 0.11$, $c_{35} = 0.03$, $c_{36} = -0.09$, $c_{44} = 1.00$, $c_{45} = 0.11$, $c_{46} = -0.07$, $c_{55} = 0.88$, $c_{56} = 0.01$, $c_{66} = 1.11$.

Figure 3 compares the errors for our three inversion scenarios. As expected, the smallest errors in the estimated stiffnesses correspond to scenario 1, for which the number of unknowns is just 21 (Table 1). Interestingly, the errors in scenarios 1 and 2 are comparable, which suggests that knowing the horizontal slownesses of S-waves is not especially important for estimating the stiffness tensor **c**. On the other hand, in scenario 3, the errors are substantially higher. Since in scenario 3 the number of unknowns is greater than the number of equations (Table 1), infinite errors (not shown) are associated with some horizontal slowness components that have to be found along with the stiffnesses.

We conclude this section by noting that the obtained results are based on analysis of the Frechèt derivative matrix, which represents the linearization of the truly nonlinear inverse problem in the vicinity of its solution. Next, we perform actual nonlinear inversion of synthetic noise-contaminated VSP data and show that the above conclusions remain qualitatively valid.

INVERSION SCHEME AND NUMERICAL RESULTS

For scenario 1, for which the horizontal slownesses of both P- and S-waves at the receiver location are known, the problem of obtaining the stiffnesses c_{ij} from equations (1) is linear. Its solution is given by

$$\mathbf{m} = \boldsymbol{\mathcal{F}}^{\dagger}\mathbf{d}, \tag{12}$$

where $\boldsymbol{\mathcal{F}}$ is the Frechèt matrix defined by equation (9).

In scenarios 2 and 3, when the inversion becomes nonlinear, we implemented the following procedure. First, given a trial stiffness tensor **c**, we minimize $\mathbf{F}^2(\mathbf{c}, \mathbf{p}^{(Q)})$ [equation (1)] with respect to the horizontal slownesses $p_1^{(Q)}$ and $p_2^{(Q)}$ at each data

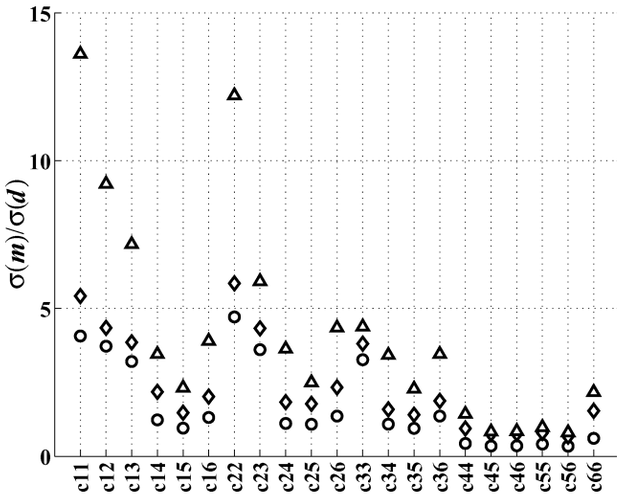

FIG. 3. Comparison of the error-amplification factors $\sigma(\mathbf{m})/\sigma(\mathbf{d})$ for inversion scenarios 1 (circles), 2 (diamonds), and 3 (triangles). As before, the data were computed at the spatial directions and for the model described in the caption of Figure 2.

point. Once the horizontal slowness components (four per data point in scenario 2 and six per point in scenario 3) are obtained, we seek a minimum of the objective function

$$\Phi(\mathbf{c}) = \sum \mathbf{F}^2\left(\mathbf{c},\ \mathbf{p}^{(Q)}\right) \tag{13}$$

with respect to $\mathbf{c}$. The summation here is performed over all data points, and the conjugate gradient method is used in both optimization steps. The main advantage of this inversion scheme is that it allows us to split the full parameter space, which includes both $\mathbf{c}$ and $\mathbf{p}^{(Q)}$, into a sequence of substantially smaller subspaces. As a result, we significantly improve computational efficiency without compromising the rate of convergence.

To test the inversion algorithm, we computed the polarization and slowness vectors in an orthorhombic model. Then, the data were contaminated with Gaussian noise that had standard deviations 2% for the slownesses and 10° for the polarization vectors. The stiffnesses have been estimated for different realizations of the noise. We did not use information about the symmetry of the model, so the data were inverted for triclinic media.

The results presented in Figure 4 (scenario 1) clearly indicate that all elements of the stiffness tensor that are strictly zero in the original orthorhombic medium are, indeed, small. Thus, knowing the symmetry of the model a priori is not needed for the inversion; the symmetry can be inferred from the results. The larger error bars for the computed stiffness coefficients c_{11}, c_{12}, and c_{22} as compared to those for c_{44} and c_{55} can be explained by the limited polar coverage of the data (up to 52° from the vertical). Note that relative errors in the estimated stiffnesses are reasonably well predicted by the above analysis of the Frechèt matrix (Figure 3).

When we follow scenario 2 to invert the stiffnesses from the same data [except for the slowness components $p_{1,n}^{(S_1)}$, $p_{2,n}^{(S_1)}$, $p_{1,n}^{(S_2)}$, and $p_{2,n}^{(S_2)}$ that now become a part of the model; compare equations (3) and (4)], we obtain less accurate results. Such loss of accuracy is predicted by the SVD analysis (compare the locations of circles and diamonds in Figure 3). The obtained estimates of stiffness coefficients can be improved by increasing the polar coverage of the data. Figure 5, where the maximum polar angle $\alpha^{(1)} = 65°$, indicates that the errors in the estimated c_{ij} become comparable to those in Figure 4, even though the horizontal slownesses of S-waves are still unknown.

The inversion following scenario 3 (Figure 6) reveals a serious deterioration in the obtained estimates. Not only do the error bars generally increase compared to those in Figure 5, but the method also fails to constrain the stiffnesses c_{11}, c_{12}, and c_{22}. Again, the reason for this can be seen in Figure 3. The

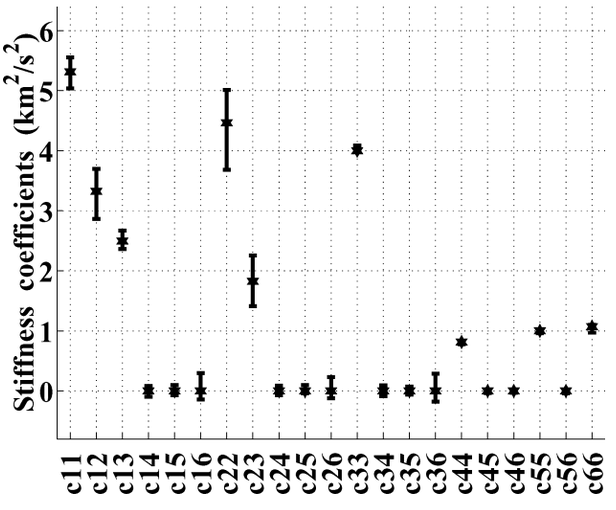

FIG. 4. Results of linear inversion (scenario 1) of polarization and slowness vectors. Stars denote the exact values of the stiffness coefficients (corresponding to an orthorhombic model), bars represent ± one standard deviation in the estimated quantities. The data were computed at 24 directions specified by four polar angles $\alpha^{(1)} = [13°,\ 26°,\ 39°,\ 52°]$ and six azimuths $\alpha^{(2)} = [0°,\ 30°,\ 60°,\ 90°,\ 120°,\ 150°]$.

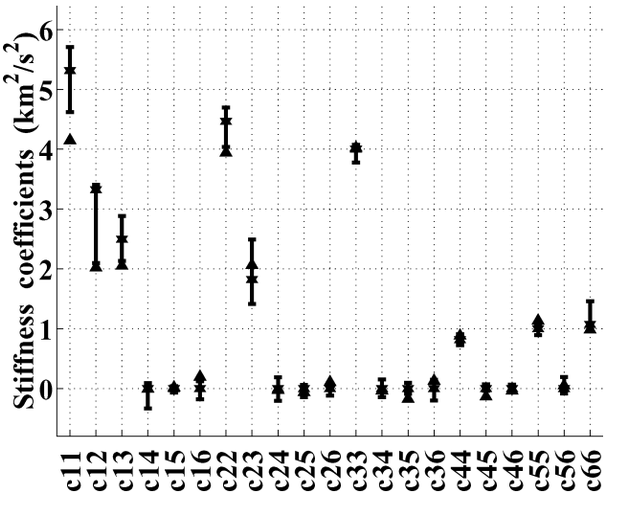

FIG. 5. Inversion following scenario 2 for the same model as that in Figure 4 but for data generated at 30 directions given by five polar angles $\alpha^{(1)} = [13°,\ 26°,\ 39°,\ 52°,\ 65°]$ and six azimuths $\alpha^{(2)} = [0°,\ 30°,\ 60°,\ 90°,\ 120°,\ 150°]$. Triangles mark the initial guesses for the components of tensor $\mathbf{c}$.

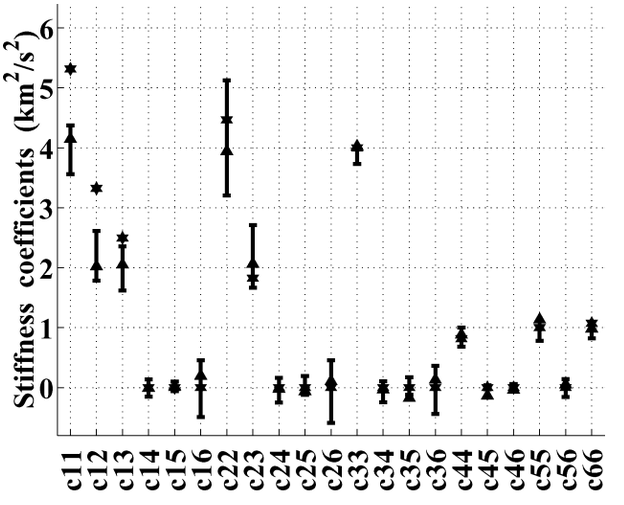

FIG. 6. Inversion of the data with the coverage described in the caption of Figure 5 following scenario 3.

standard deviations in c_{11}, c_{12}, and c_{22} predicted by the SVD are so large that any reasonable values of those elastic coefficients fit the data. As a consequence, the estimates of c_{11} and c_{12} stay close to the corresponding initial guesses (triangles in Figure 6), and c_{22} has a large variability.

So far, we avoided making any assumptions about the type of anisotropy of the model and attempted to estimate all 21 stiffness coefficients. Let us now reduce the number of unknown stiffnesses to nine by assuming the model to be orthorhombic with a known orientation of the symmetry planes. Figure 7 shows the inverted nonzero stiffness coefficients following scenario 2. Comparing Figures 5 and 7, we observe some decrease of the error bars. Although the symmetry is clearly helpful for the inversion, Figures 5 and 7 indicate that it does not lead to significant improvement of the results.

FIELD-DATA EXAMPLE

Next, we apply our inversion scheme to a 3D walkaway VSP data set acquired in Vacuum field, Lea County, New Mexico. The data were recorded by a string of 10 three-component geophones placed in a vertical well with a 15-m depth increment between 304.8 and 439.8 m. Vertical and horizontal vibrators at about 250 shotpoints uniformly distributed around the borehole with the offsets reaching 510 m were used to excite P- and S-waves, respectively. The details of data acquisition can be found in Michaud (2001).

Estimation of polarization and slowness vectors

The initial data processing was performed by Michaud (2001). She applied the technique of DiSeina et al. (1984) to obtain the P-wave polarization vectors and used Alford (1986) rotation of the sources and receivers to separate two shear waves and find their polarization directions. The results for the receiver at depth 304.8 m are shown in Figures 8a–c.

The analysis of traveltimes $t^{(Q)}$ picked for P-, S_1-, and S_2-arrivals reveals the following: (1) traveltime minima $t_0^{(Q)}$ correspond to the borehole location for all receiver positions,

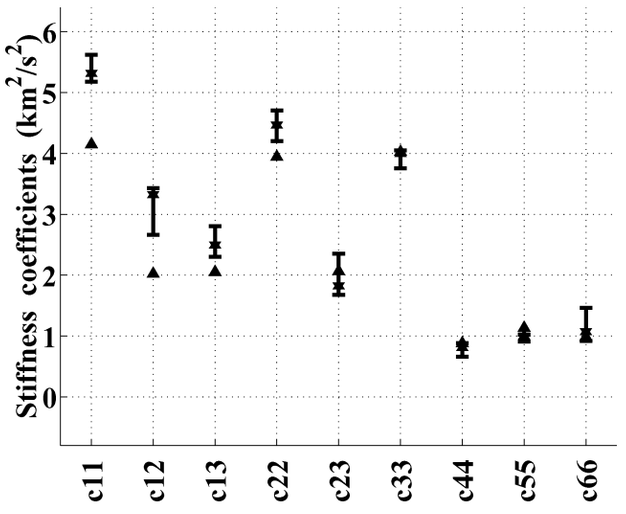

FIG. 7. Same as Figure 5 but assuming that the model is orthorhombic with known orientation of the symmetry planes.

(2) traveltimes are symmetric with respect to the well. Based on these observations and to reduce the influence of noise on traveltime picks, we have chosen to approximate the squared traveltimes $t^{(Q)}$ by a 2D Taylor series,

$$\left[t^{(Q)}(\mathbf{x})\right]^2=\left[t_0^{(Q)}(x_3)\right]^2+\sum_{j_1,j_2=1}^{2}a_{j_1j_2}^{(Q)}(x_3)x_{j_1}x_{j_2}+\sum_{j_1,j_2,j_3,j_4=1}^{2}b_{j_1j_2j_3j_4}^{(Q)}(x_3)x_{j_1}x_{j_2}x_{j_3}x_{j_4},\quad(14)$$
$$(Q=\mathrm{P},\ \mathrm{S}_1,\ \mathrm{S}_2).$$

Here, the traveltimes $t^{(Q)}(\mathbf{x})$ are written in a Cartesian coordinate frame $[x_1,\ x_2,\ x_3]$ with the origin at the borehole location and the axes x_1, x_2, and x_3 oriented in the east-west, north-south, and vertical directions, respectively; x_1 and x_2 denote the source coordinates, x_3 is the receiver depth. The coefficients $a_{j_1j_2}^{(Q)}(x_3)$ and $b_{j_1j_2j_3j_4}^{(Q)}(x_3)$ in equation (14) are symmetric with respect to any pair of their indexes. We find the quantities $[t_0^{(Q)}(x_3)]^2$, $a_{j_1j_2}^{(Q)}(x_3)$, and $b_{i_1i_2i_3i_4}^{(Q)}(x_3)$ at all receiver levels x_3 using the least-squares method.

Next, we compute the slowness vectors according to their definition,

$$p_i^{(Q)}\equiv\frac{\partial t^{(Q)}}{\partial x_i}.\quad(15)$$

The result of this calculation for receiver at depth 304.8 is shown in Figures 8d–f. Note that the polar coverage of the data is extremely good. Since the polar angles reach 75°–80°, we might expect a comparable accuracy in the estimated stiffness coefficients that govern wave propagation in both near-vertical and near-horizontal directions.

Inversion for stiffness coefficients

The studies done by Roche (1997) and the observed traveltime symmetry,

$$t^{(Q)}(x_1,\ x_2,\ x_3)=t^{(Q)}(-x_1,\ -x_2,\ x_3),\quad(16)$$

indicate that the subsurface structure in the vicinity of the well is close to horizontally layered with almost no lateral velocity variations. This enables us to use the linear inversion strategy of scenario 1. We make no assumption about the medium symmetry and invert the data for a triclinic model. To obtain a suite of inversion results rather than a single model, we contaminate the polarizations and slownesses (such as those shown in Figure 8) with Gaussian noise. According to the estimates of Michaud (2001), the errors in the polarization and slowness vectors are 12° and 5%, respectively. We impose these values as the corresponding standard deviations.

It turns out that the inverted stiffness coefficients (Figure 9) are accurately described by an azimuthally rotated orthorhombic medium. [In fact, we also performed the inversion following scenario 2 that does not use shear-wave horizontal slowness components. Starting from an isotropic initial model, we obtained the stiffnesses (not shown) similar to those displayed in Figure 9.] The local x_3'-axis of this orthorombic medium has a tilt of approximately 4° with respect to the vertical and east-west azimuth. This tilt is statistically insignificant, so we can

assume that the model has a horizontal symmetry plane. The local x_1'-axis points at 25°SE; the 95% confidence interval for this value is ±15°. The velocities (along the x_3'-axis) of the obtained orthorhombic model and its anisotropic coefficients (Tsvankin, 1997) are shown in Figure 10. Our model correctly reproduces the direction of the S-wave polarization vectors at small offsets (Figures 8b,c) and the features displayed on the slowness plots (Figures 8d–f). In particular, the shear-wave splitting coefficient $\gamma^{(S)} = (\gamma^{(2)} - \gamma^{(1)})/(1 + 2\gamma^{(2)}) \approx 0.10$ matches that inferred from Figures 8e,f. Also the elongation of the P-wave slowness contours in approximately southeast-northwest direction (Figure 8d) corresponds to the inequality $\delta^{(2)} > \delta^{(1)}$ between two of the δ-coefficients [equation (20) in Grechka and Tsvankin (1999)].

Some insight into the goodness-of-fit of the data can be gained from the residuals $\Delta A_i^{(Q)}$ and $\Delta p_3^{(Q)}$ plotted in Figure 11. We observe that our best-fit model is quite successful in predicting the P- and S_1-wave slownesses (Figures 11d,e), whereas the residuals $\Delta p_3^{(S_2)}$ have substantial bias (Figure 11f). Likewise, the P-wave polarizations (Figure 11a) are well described, whereas the polarizations of shear modes are relatively poor (Figures 11b,c). Since the residuals in Figures 11b,c,f display systematic patterns, it appears that errors in the inversion are mainly caused by the S-wave polarizations and slownesses. In

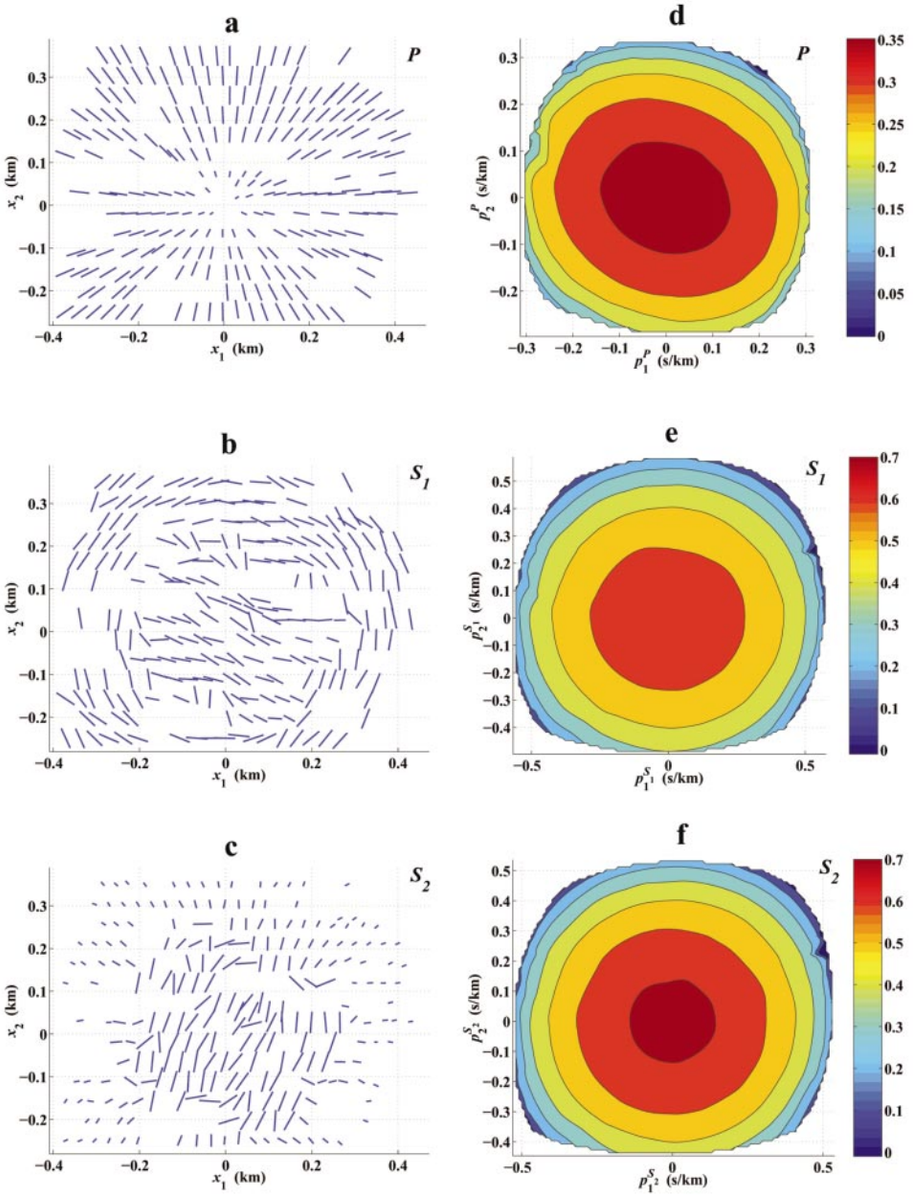

FIG. 8. (a, b, c) Horizontal projections of the polarization vectors (longer ticks correspond to waves polarized almost horizontally) and (d, e, f) vertical slowness components $p_3^{(Q)}$ ($p_1^{(Q)}$, $p_2^{(Q)}$) (in s/km) of P-, S_1-, and S_2-waves, respectively, for a receiver at depth 304.8 m. The well is located at $x_1 = x_2 = 0$.

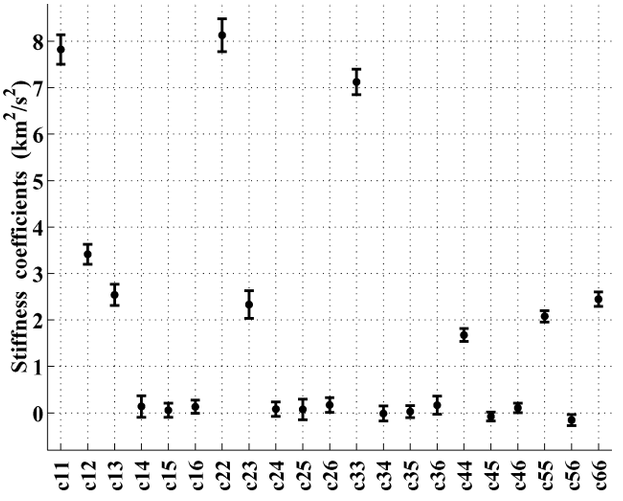

FIG. 9. Inverted stiffness coefficients of triclinic media. Dots indicate mean values, bars correspond to the 95% confidence intervals resulting from adding Gaussian noise with the standard deviation equal to 12° for polarization vectors and 5% for the slownesses.

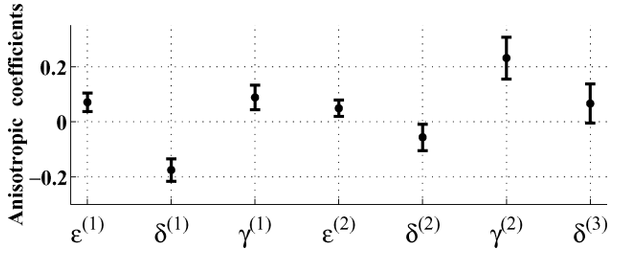

FIG. 10. Tsvankin's (1997) anisotropic coefficients for the estimated orthorhombic media. As in Figure 9, dots indicate the mean values, and bars correspond to the 95% confidence intervals. The vertical velocities for the obtained models are $V_{P0} = 2.66 \pm 0.05$ km/s and $V_{S0} = 1.44 \pm 0.04$ km/s (not shown).

fact, this observation could have been expected because the vectors $\mathbf{A}^{(S_1)}$ and $\mathbf{A}^{(S_2)}$ were obtained by applying Alford rotation, which implies the orthogonality $\mathbf{A}^{(S_1)} \perp \mathbf{A}^{(S_2)}$. At large incidence angles, however, the vectors $\mathbf{A}^{(S_1)}$ and $\mathbf{A}^{(S_2)}$ are not orthogonal to each other, as can be verified from the corresponding slowness vectors $\mathbf{p}^{(S_1)}$ and $\mathbf{p}^{(S_2)}$ (Figures 8e,f), which are not parallel. This inconsistency propagates through the inversion scheme (which tries to fit all the data simultaneously) and contributes to the overall error.

Even given the possible errors, our results agree with the existing studies of Vacuum field. For instance, Mattocks (1998) examined the polarization of S-waves and the focusing of shear-wave energy, and concluded that the overburden (shallow 300 m) of Vacuum field has orthorhombic symmetry. In addition, the study of borehole breakouts performed by Scuta (1997) resulted in the estimate of azimuth of the maximum horizontal stress of about 32° southeast.

DISCUSSION AND CONCLUSIONS

The feasibility of estimating the full stiffness tensor **c** from multicomponent, multiazimuth, walkaway VSP data depends on several factors. First, the overburden complexity determines our ability to estimate the horizontal slowness components p_1 and p_2 at the geophone levels. When such estimates of p_1 and p_2 cannot be made (scenario 3), the large error bars in the inverted stiffnesses render them almost useless. We showed that knowing the horizontal slowness components of only P-waves (scenario 2) makes the inversion for all c_{ij} feasible. When the components of p_1 and p_2 of the shear-waves can be also measured (scenario 1), the stability of the inverted stiffness coefficients increases.

Another factor that governs the accuracy of any given c_{ij} is the data coverage. Since different stiffness coefficients influence wave propagation for different ranges of polar and azimuthal angles, full coverage may be needed to obtain all c_{ij} with a comparable accuracy. In practice, however, we may expect to have a much better coverage in near-vertical directions than near the horizontal. As a result, errors in c_{11}, c_{12}, c_{22}, and c_{66} are usually greater than those in c_{33}, c_{44}, and c_{55}. Our numerical tests confirm that.

In general, the accuracy of inverted stiffness coefficients increases if the medium has a known higher symmetry. This obviously relates to the number of unknown quantities one attempts to estimate from a given data set. We have found, though, that the gain in accuracy is not substantial enough to make the assumption of a particular symmetry absolutely necessary. On the other hand, allowing for the most general triclinic anisotropy offers the potential of recognizing the medium symmetry from the inversion results in contrast to assuming it a priori.

The presented case study substantiates the last point. We estimated the stiffness tensor of a triclinic model by fitting both the polarization and slowness vectors of the P- and two split S-waves. We also showed that the obtained stiffnesses are close to those describing an azimuthally rotated orthorhombic model. The orientation of its symmetry planes fits a number of independent observations and seems to relate to the subsurface stresses.

ACKNOWLEDGMENTS

We are grateful to Ilya Tsvankin and Ken Larner [Center for Wave Phenomena (CWP)] for fruitful discussions, Tom Davis [Reservoir Characterization Project at Colorado School of Mines (CSM)] for providing the data, and Joe Dellinger (BP) for letting us use his code that approximates a given triclinic model with a higher symmetry one. We thank Joe Dellinger, Ivan Pšenčík, and Jerry Schuster for reviewing our manuscript. P. Dewangan was supported by the members of the Consortium Project on Seismic Inverse Methods for Complex Structures at CWP, CSM. V. Grechka thanks Shell International E & P for permission to publish the paper.

REFERENCES

Alford, R. M., 1986, Shear data in the presence of azimuthal anisotropy: 56th Ann. Internat. Mtg., Soc. Expl. Geophys., Expanded Abstracts, 476–479.

Bakulin, A., Grechka, V., and Tsvankin, I., 2000a, Estimation of fracture parameters from reflection seismic data. Part II: Fractured models with orthorhombic symmetry: Geophysics, **65**, 1803–1817.

——— 2000b, Estimation of fracture parameters from reflection seismic data. Part III: Fractured models with monoclinic symmetry: Geophysics, **65**, 1818–1830.

Bakulin, A., Slater, C., Bunain, H., Grechka, V., 2000c, Estimation of azimuthal anisotropy and fracture parameters from multiazimuthal

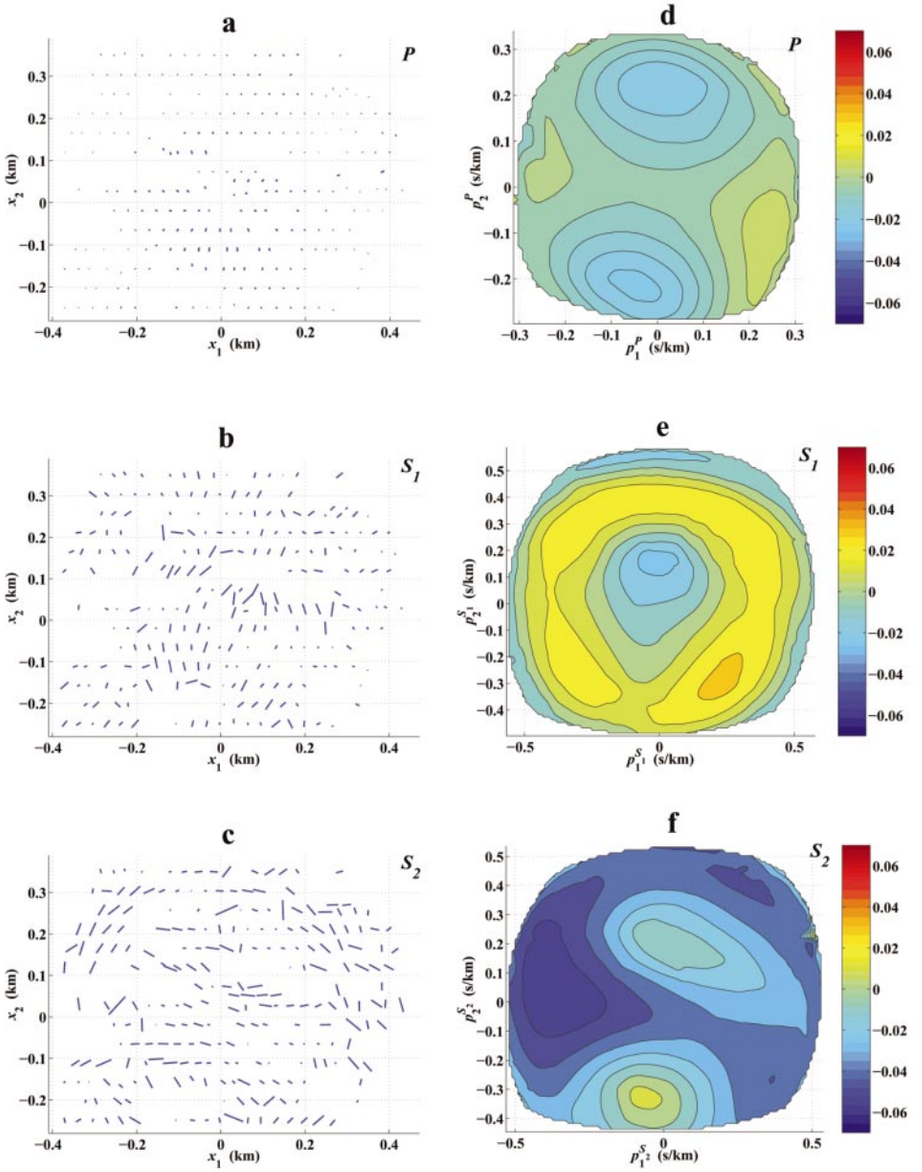

FIG. 11. (a, b, c) Residuals of the horizontal components of the polarization vectors $\Delta A_i^{(Q)} = A_i^{(Q)\text{meas}} - A_i^{(Q)\text{comp}} (i = 1, 2)$ and (d, e, f) the vertical slowness components $\Delta p_3^{(Q)} = p_3^{(Q)\text{meas}} - p_3^{(Q)\text{comp}}$ (in s/km) of the P-, S_1-, and S_2-waves, respectively. The computed quantities correspond to the triclinic model marked by dots in Figure 9. The scale for polarizations is the same as that in Figure 8.

walkaway VSP in the presence of lateral heterogeneity: 70th Ann. Internat. Mtg., Soc. Expl. Geophys., Expanded Abstracts, 1405–1408.

Dellinger, J. A., Nolte, B., and Etgen, J. T., 2001, Alford rotation, ray theory, and crossed-dipole geometry: Geophysics, **66**, 637–647.

DiSeina, J. P., Gaiser, J. E., and Corrigan, D., 1984, Horizontal components and shear wave analysis of three-component VSP data, in Toksoz, M. N., and Steward, R. R., Eds., Vertical seismic profiling, Part B: Advanced concepts: Geophysical Press, 177–188.

Gaiser, J. E., 1990, Transversely isotropic phase velocity analysis from slowness estimates: J. Geophys. Res., **95**, 241–254.

Grechka, V., Bakulin, A., and Tsvankin, I., 2001, Seismic characterization of vertical fractures described as general linear-slip interfaces: 63rd Conf., Eur. Assn. Geosci. Eng., Extended Abstracts, P-201.

Grechka, V., and Tsvankin, I., 1999, 3-D moveout velocity analysis and parameter estimation for orthorhombic media: Geophysics, **64**, 820–837.

Horne, S., and Leaney, S., 2000, Polarization and slowness component inversion for TI anisotropy: Geophys. Prosp., **48**, 779–788.

Mattocks, B., 1998, Borehole geophysical investigation of seismic anisotropy at Vacuum field, Lea County, New Mexico: Ph.D. thesis, Colorado School of Mines.

Michaud, G., 2001, Multicomponent borehole seismic monitoring of a pilot CO_2 flood: Ph.D. thesis, Colorado School of Mines.

Miller, D. E., and Spencer, C., 1994, An exact inversion for anisotropic moduli from phase slowness data: J. Geophys. Res., **99**, 651–657.

Press, W. H., Flannery, B. P., Teukolsky, S. A., and Vetterling, W. T., 1987, Numerical recipes: The art of scientific computing: Cambridge University Press.

Roche, S., 1997, Time-lapse, multicomponent, three-dimensional seismic characterization of a San Andres shallow shelf carbonate reservoir, Vacuum field, Lea County, New Mexico: Ph.D. thesis, Colorado School of Mines.
Sayers, C. M., 1997, Determination of anisotropic velocity models from walkaway VSP data acquired in the presence of dip: Geophysics, **62**, 723–729.
Scuta, M., 1997, 3-D geological characterization of Central Vacuum unit, Lea County, New Mexico: Ph.D. thesis, Colorado School of Mines.
Tsvankin, I., 1997, Anisotropic parameters and P-wave velocity for orthorhombic media: Geophysics, **62**, 1292–1309.
——— 2001, Seismic signatures and analysis of reflection data in anisotropic media: Pergamon.
Zheng, X., and Pšenčík, I., 2002, Local determination of weak anisotropy parameters from qP-wave slowness and particle motion measurements: Pure Appl. Geophys., **159**, 1881–1905.